Effects of an additional conduction band on the singlet-antiferromagnet competition in the periodic Anderson model

Wenjian Hu, Richard T. Scalettar, Edwin W. Huang, and Brian Moritz

Phys. Rev. B **95**, 235122 — Published 12 June 2017

DOI: 10.1103/PhysRevB.95.235122

Effects of an Additional Conduction Band on Singlet-Antiferromagnet Competition in the Periodic Anderson Model

Wenjian Hu[1], Richard T. Scalettar[1], Edwin W. Huang[2,3], and Brian Moritz[3,4]
[1]*Department of Physics, University of California Davis, Davis, CA 95616, USA*
[2]*Department of Physics, Stanford University, Stanford, CA 94305, USA*
[3]*Stanford Institute for Materials and Energy Sciences, SLAC National Accelerator Laboratory and Stanford University, Menlo Park, CA 94025, USA*
[4]*Department of Physics and Astrophysics, University of North Dakota, Grand Forks, ND 58202, USA*

The competition between antiferromagnetic (AF) order and singlet formation is a central phenomenon of the Kondo and Periodic Anderson Hamiltonians, and of the heavy fermion materials they describe. In this paper, we explore the effects of an additional conduction band on magnetism in these models, and, specifically, on changes in the AF-singlet quantum critical point (QCP) and the one particle and spin spectral functions. To understand the magnetic phase transition qualitatively, we first carry out a self-consistent mean field theory (MFT). The basic conclusion is that, at half-filling, the coupling to the additional band stabilizes the AF phase to larger f d hybridization V in the PAM. We also explore the possibility of competing ferromagnetic phases when this conduction band is doped away from half-filling. We next employ Quantum Monte Carlo (QMC) which, in combination with finite size scaling, allows us to evaluate the position of the QCP using an exact treatment of the interactions. This approach confirms the stabilization of AF order, which occurs through an enhancement of the Ruderman-Kittel-Kasuya-Yosida (RKKY) interaction. QMC results for the spectral function $A(\mathbf{q},\omega)$ and dynamic spin structure factor $\chi(\mathbf{q},\omega)$ yield additional insight into the AF-singlet competition and the low temperature phases.

I. INTRODUCTION

The periodic Anderson Model (PAM) describes the hybridization between mobile (d band) free electrons in a metal with strongly correlated f electrons. The PAM has been extensively studied since its first introduction[1], and can successfully account for a variety of remarkable f-electron (rare-earth and actinide) phenomena including heavy-fermion physics[2–6], valence fluctuations[7,8], volume collapse transitions[9–16] and unconventional superconductivity[17].

At low temperatures, as the hybridization strength is varied in the PAM, there is a competition between the RKKY interaction[18–20], which favors magnetically ordered f band local moments, and the Kondo effect[21,22], which screens the local moments and induces singlet states. Kondo screening can also occur at the interface between metallic and strongly correlated materials[23,24], a situation which has given rise to additional theoretical and numerical investigation of the PAM and its geometrical variants[25–27]. Here the metallic band is viewed as arising from material on one side of an interface, and the correlated band describes the other side of the interface, as opposed to originating from strongly and weakly correlated orbitals of atoms in a single, homogeneous material.

A natural generalization of models which couple a single conduction band to localized, magnetic, orbitals is to consider similar physics when several conduction bands are present. The new qualitative physics to be explored is how the third band, and the resulting imbalance between the numbers of conduction and loacalized electrons, alters the strong correlation phenomena of the two band PAM: RKKY-induced AF order at weak V, the nature of the Kondo gap at strong V, and, finally, the position of the AF-singlet transition between these limits.

Besides these interesting fundamental questions, such a model is also worthy of investigation as a first step towards experiments[28] on f-electron superlattices like $CeIn_3$(n)/$LaIn_3$(m). In these systems, by varying the thicknesses n, m of the different materials, the effective dimensionality can be tuned, and hence the $2D$-$3D$ crossover of Kondo physics and AF order.

Recent theoretical investigations of the effect of immersing a Kondo insulator, or a superlattice thereof, in a 3D metal has been undertaken by Peters *et al.*[29]. The focus there was on the evolution of the density of states $\rho(\omega)$ and, especially, features like the Fermi level hybridization gap of the Kondo sheet. A key conclusion is that the Kondo gap is modified to a pseudogap, with quadratically vanishing $\rho(\omega)$ from coupling to the metallic layer, and that the 3D $\rho(\omega)$ of the metallic layer adjacent to the Kondo layer develops 2D features. Changes to $\rho(\omega = 0)$ in the singlet phase will be a key feature of our results here.

A bilayer heavy fermion system comprising a Kondo insulator (KI), represented by a symmetric PAM, coupled to a simple metal (M) has been proposed and studied employing the framework of DMFT[6] at half-filling. The main goal of the work was to determine the ground state phase diagram from a Kondo screened Fermi liquid to a Mott insulating phase as a function of interaction strength and interlayer coupling. More generally, the possibility of the coexistence of spectral functions with distinct behaviors near the Fermi surface, despite the presence of interband hybridization, is the topic of studies of orbitally selective transitions[30,31].

While we focus here on the influence of an additional metallic band on the properties of the PAM, similar extensions to include electron-phonon coupling[32], dilution[33], and f-electron hybridization[34] have similarly explored the ways in which AF-singlet competition can be influenced by the inclusion of further energy scales and degrees of freedom in the Hamiltonian.

In this paper, we employ the determinant quantum Monte Carlo (DQMC) method[35,36], which provides an approximation-free solution to strong correlations, to study the magnetic structure of the bilayer KI-M system. By finite size scaling, we reliably extract the AF order parameter as a function of the KI hybridization strength V, and then build up the magnetic phase diagram in the $V - t'$ plane for a representative potential $U_f = 4$. To understand more precisely the role of nonzero t', we begin with a redetermination of the quantum critical point (QCP) of the AF-singlet phase transition of the half-filled PAM, the $t' = 0$ limit, with higher accuracy than in previous literature[37]. The DQMC work is mainly focused on the particle-hole symmetric (half-filled) limit where there is no sign problem in the simulation. We also implemented a mean-field theory (MFT) calculation bothe at and away from half-filling as a supplement to DQMC. Our work is distinguished from previous work[6,29] by its consideration of a PAM rather than a coupling to local (Kondo) spins, and its treatment of intersite magnetic correlations which are suppressed in the paramagnetic DMFT used in earlier work.

II. MODEL AND METHODS

We consider the bilayer KI-M Hamiltonian on a square lattice,

$$\begin{aligned} H = & -t \sum_{<\mathbf{i},\mathbf{j}>\sigma} (c^\dagger_{\mathbf{i}\sigma} c_{\mathbf{j}\sigma} + c^\dagger_{\mathbf{j}\sigma} c_{\mathbf{i}\sigma}) + \epsilon^c \sum_{\mathbf{i}\sigma} n^c_{\mathbf{i}\sigma} \\ & - t \sum_{<\mathbf{i},\mathbf{j}>\sigma} (d^\dagger_{\mathbf{i}\sigma} d_{\mathbf{j}\sigma} + d^\dagger_{\mathbf{j}\sigma} d_{\mathbf{i}\sigma}) + \epsilon^d \sum_{\mathbf{i}\sigma} n^d_{\mathbf{i}\sigma} \\ & + U_f \sum_{\mathbf{i}} (n^f_{\mathbf{i}\uparrow} - \frac{1}{2})(n^f_{\mathbf{i}\downarrow} - \frac{1}{2}) + \epsilon^f \sum_{\mathbf{i}\sigma} n^f_{\mathbf{i}\sigma} \\ & - t' \sum_{\mathbf{i}\sigma} (c^\dagger_{\mathbf{i}\sigma} d_{\mathbf{i}\sigma} + d^\dagger_{\mathbf{i}\sigma} c_{\mathbf{i}\sigma}) - V \sum_{\mathbf{i}\sigma} (d^\dagger_{\mathbf{i}\sigma} f_{\mathbf{i}\sigma} + f^\dagger_{\mathbf{i}\sigma} d_{\mathbf{i}\sigma}) \quad (1) \end{aligned}$$

t is the intralayer hopping parameter, which, for simplicity, we chose to be the same in the uncorrelated c and d bands. t' is the interlayer hopping parameter between the c, d bands. V is the hybridization strength between the d, f bands. U_f is the Coulomb repulsion in the f band. Finally, ϵ^α are the orbital energies of the $\alpha = c, d$, and f bands, and $n^\alpha_{\mathbf{i}\sigma} \equiv \alpha^\dagger_{\mathbf{i}\sigma} \alpha_{\mathbf{i}\sigma}$ are the density operators. The model is shown pictorially in Fig. 1, where f and d bands belong to the KI layer, and c band belongs to the metal layer. Within the KI formed by the d and f bands, V controls the competition between antiferromagnetic (AF) and singlet phases.

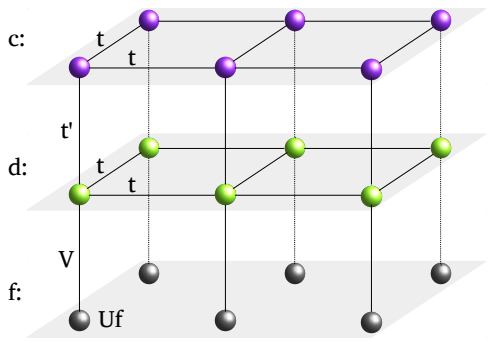

FIG. 1: Three band system with f and d bands comprising the KI (PAM) layer coupling to an additional c (metallic) layer. These KI and metal are coupled through an interlayer hopping parameter t'. Our primary tuning parameter will be the hybridization V within the KI.

In this work, we set $t = 1$ as our energy scale and mainly consider the particle-hole symmetric limit where $\epsilon^\alpha = 0$, so each of the three bands is individually half-filled. We also implement the MFT calculation away from half-filling.

At half-filling, the Hamiltonian can be solved exactly in the noninteracting limit ($U_f = 0$). Unlike the PAM in which V opens a gap at half-filling and which hence is a band insulator there, the KI-M system is metallic at half-filling. This follows from the fact that the Hamiltonian has an odd number of bands (three): the Fermi level lies in the middle of the central band.

This metallic character at half-filling can be made more precise by going to momentum space $\alpha^\dagger_{\mathbf{k}\sigma} = (1/\sqrt{N}) \sum_{\mathbf{l}} e^{i\mathbf{k}\mathbf{l}} \alpha^\dagger_{\mathbf{l}\sigma}$ for each of the three bands $\alpha = c, d, f$.

$$H = \sum_{\mathbf{k}\sigma} \begin{bmatrix} c^\dagger_{\mathbf{k}\sigma} & d^\dagger_{\mathbf{k}\sigma} & f^\dagger_{\mathbf{k}\sigma} \end{bmatrix} \begin{bmatrix} \epsilon_{\mathbf{k}} & -t' & 0 \\ -t' & \epsilon_{\mathbf{k}} & -V \\ 0 & -V & 0 \end{bmatrix} \begin{bmatrix} c_{\mathbf{k}\sigma} \\ d_{\mathbf{k}\sigma} \\ f_{\mathbf{k}\sigma} \end{bmatrix} \quad (2)$$

Here $\epsilon_{\mathbf{k}} = -2t(\cos(k_x) + \cos(k_y))$. Diagonalizing the Hamiltonian Eq. 2 yields the three energy bands. In general, these bands cross and, at $\epsilon^\alpha = 0$, are all partially filled. However, in certain limits, e.g. $V = 0$ and $t' > 4t$, band gaps are present. Even so, in these situations the central band is half-filled and the system remains metallic.

The focus of our work will be the implications of the additional metallic (c) band on the competition between the RKKY interaction-induced AF and the Kondo regime of screened singlets, both central to the behavior of heavy-fermion materials[2–4] and captured in the solution of the PAM ($t' = 0$). A natural expectation is that, with the increase of t', the RKKY interaction between the local f moments is enhanced, due to the additional conduction band channels, while the Kondo energy scale, set by V and U_f, remains roughly fixed. This should lead

to an overall movement of the quantum critical point to larger values of V.

To understand the precise effect of t' on the AF-singlet transition, we first carried out a self-consistent mean field theory (MFT). We then turned to a more exact, DQMC solution.

III. RESULTS: MEAN FIELD THEORY

Together with Kondo phases, ferromagnetic, antiferroferromagnetic and mixed order are all possible in the PAM and related Hamiltonians[38,39]. In the MFT treatment presented here, we thus consider three possible phases, the AF phase, the ferromagnetic (F) phase and the singlet phase. The AF MFT *ansatz* is

$$\langle n^f_{\mathbf{l}\sigma}\rangle = \frac{n_f}{2} + \frac{\sigma m_f(-1)^{\mathbf{l}}}{2} \tag{3}$$

where σ is spin up ($\uparrow$) or spin down ($\downarrow$) and m_f is the f band AF order parameter. While the F MFT *ansatz* is

$$\langle n^f_{\mathbf{l}\sigma}\rangle = \frac{n_f}{2} + \frac{\sigma m_f}{2} \tag{4}$$

where σ follows the same definition and m_f is the f band ferromagnetic order parameter. In order to fix the particle densities n_c, n_d and n_f, the terms $Nn_c\epsilon^c$, $Nn_d\epsilon^d$ and $Nn_f\epsilon^f$ must be subtracted from the original Hamiltonian, Eq. 1 reported in Ref.[40].

The AF MF decoupling of the interaction then gives a quadratic Hamiltonian in which momenta $\mathbf{k}$ and $\mathbf{k}$ - $\mathbf{Q}$ (where $\mathbf{Q} = (\pi, \pi)$) are coupled, resulting in

$$H_{AF} = \frac{1}{2}\sum_{\mathbf{k}\sigma} v^\dagger_{\mathbf{k}\sigma} M^{AF}_{\mathbf{k}\sigma} v_{\mathbf{k}\sigma} + \frac{NU_f(m_f^2+n_f^2-1)}{4} - Nn_c\epsilon^c - Nn_d\epsilon^d - Nn_f\epsilon^f \tag{5}$$

where $v^\dagger_{\mathbf{k}\sigma} = \left[\begin{array}{cccccc} c^\dagger_{\mathbf{k}\sigma} & d^\dagger_{\mathbf{k}\sigma} & f^\dagger_{\mathbf{k}\sigma} & c^\dagger_{\mathbf{k}-\mathbf{Q},\sigma} & d^\dagger_{\mathbf{k}-\mathbf{Q},\sigma} & f^\dagger_{\mathbf{k}-\mathbf{Q},\sigma}\end{array}\right]$,

$$M^{AF}_{\mathbf{k}\sigma} = \begin{bmatrix} \eta^c_{\mathbf{k}} & -t' & 0 & 0 & 0 & 0 \\ -t' & \eta^d_{\mathbf{k}} & -V & 0 & 0 & 0 \\ 0 & -V & \eta^f_{\mathbf{k}} & 0 & 0 & -\frac{\sigma m_f U_f}{2} \\ 0 & 0 & 0 & \eta^c_{\mathbf{k}-\mathbf{Q}} & -t' & 0 \\ 0 & 0 & 0 & -t' & \eta^d_{\mathbf{k}-\mathbf{Q}} & -V \\ 0 & 0 & -\frac{\sigma m_f U_f}{2} & 0 & -V & \eta^f_{\mathbf{k}-\mathbf{Q}} \end{bmatrix}.$$

In $M^{AF}_{\mathbf{k}\sigma}$, $\eta^c_{\mathbf{k}}$, $\eta^d_{\mathbf{k}}$ and $\eta^f_{\mathbf{k}}$ stand for $\epsilon_{\mathbf{k}}+\epsilon^c$, $\epsilon_{\mathbf{k}}+\epsilon^d$ and $(\frac{n_f}{2}-\frac{1}{2})U_f+\epsilon^f$ respectively.

On the other hand, the F MF decoupling leads to

$$H_F = \sum_{\mathbf{k}\sigma} u^\dagger_{\mathbf{k}\sigma} M^F_{\mathbf{k}\sigma} u_{\mathbf{k}\sigma} + \frac{NU_f(m_f^2+n_f^2-1)}{4} - Nn_c\epsilon^c - Nn_d\epsilon^d - Nn_f\epsilon^f \tag{6}$$

where $u^\dagger_{\mathbf{k}\sigma}$ stands for $\left[\begin{array}{ccc} c^\dagger_{\mathbf{k}\sigma} & d^\dagger_{\mathbf{k}\sigma} & f^\dagger_{\mathbf{k}\sigma}\end{array}\right]$ and the matrix is

$$M^F_{\mathbf{k}\sigma} = \begin{bmatrix} \epsilon_{\mathbf{k}}+\epsilon^c & -t' & 0 \\ -t' & \epsilon_{\mathbf{k}}+\epsilon^d & -V \\ 0 & -V & (\frac{n_f}{2}-\frac{1}{2}-\frac{\sigma m_f}{2})U_f+\epsilon^f \end{bmatrix}.$$

Hence, m_f, ϵ^c, ϵ^d, ϵ^f and the corresponding MFT phase boundary, are computed self-consistently by minimizing the total ground state energy E

$$\left\langle \frac{\partial E}{\partial m_f}\right\rangle = \left\langle \frac{\partial E}{\partial \epsilon^c}\right\rangle = \left\langle \frac{\partial E}{\partial \epsilon^d}\right\rangle = \left\langle \frac{\partial E}{\partial \epsilon^f}\right\rangle = 0. \tag{7}$$

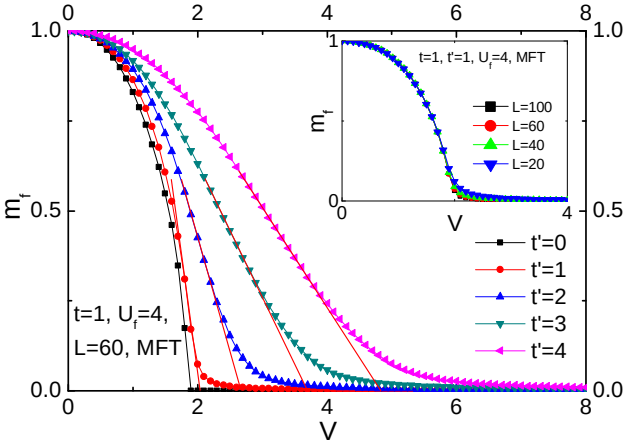

FIG. 2: MFT results for the AF order parameter m_f as a function of V for several KI-M hybridizations, $t' = 0, 1, 2, 3, 4$. Each band is fixed at half-filling. The on-site interaction in the KI, $U_f = 4$, is fixed. At $t' = 0$, where the system is insulating in the non-interacting limit, the order parameter rises from zero steeply, i.e. with the expected exponent $\beta = 1/2$ for $V < V_c$. For $t' \neq 0$, m_f exhibits a more gradual behavior. This smoother cross-over is a consequence of the diverging density of states at the Fermi surface, and reflects the persistence of AF order at large V. A 'cross-over value' V_c is identified as described in the text. Calculations shown are for lattice sizes of linear extent $L = 60$, and verified to have converged. (See inset.)

We first explore the AF MFT *ansatz* at half-filling. Results for m_f as a function of V for different couplings t' of the KI to the metal are shown in Fig. 2. A sharp QCP is evident at $t' = 0$ whose location agrees with previous work[37]. The evolution of $m_f(V)$ is smoother for $t' \neq 0$. This difference is associated with the fact that at $t' = 0$ the KI is a band insulator in the noninteracting limit, whereas, as discussed in the previous section, the KI-M model is metallic. In fact, the density of states $N(E)$ has a van-Hove singularity at the half-filled Fermi surface $E_{\mathbf{k}} = 0$, for all V with $t' \neq 0$, as also occurs in the square lattice half-filled Hubbard model. In an expansion of the free energy, $F(m_f)$ picks up a $|m_f|$ contribution from these $E_{\mathbf{k}} = 0$ modes, which persists in the thermodynamic limit owing to the divergence of

$N(E=0)$. This effect pushes V_c out to $V=\infty$ in mean field theory: AF order persists for all hybridization strengths.

Nevertheless, a cross-over V_c is still evident in Fig. 2, especially for modest t'. We assign a quantitive value by choosing the point of $m_f(V)$ of largest slope, and extrapolating linearly to $m_f=0$ as shown. These cross-over values for V_c will be compared with the critical hybridization obtained by DQMC in the following section.

To determine the ground state phase away from half-filling, we compare results from both the AF MFT *ansatz* and the F MFT *ansatz*, as shown in Fig. 3. We denote the corresponding ground state energies E_{AF} (E_F) and, for the singlet (paramagnetic) phase, E_S. In Fig. 3 (a), $E_{AF}-E_S$ and E_F-E_S are shown as a function of the density n_c with fixed $n_d=1$, $n_f=1$, that is, by doping the additional conduction band. We have chosen $t'=1$, $V=1$, $U_f=4$ and $L=200$. For these parameters, E_{AF} is always lowest for all dencities n_c. In Fig. 3(b), the optimal m_f from the AF MFT *ansatz* (denoted as m_f^{AF}) and the optimal m_f from the F MFT *ansatz* (denoted as m_f^F) are shown as a function of density n_c. Since the ground state phase is AF, red triangular data characterizes the behaviour of the ground state order parameter. While n_c is varied greatly from 0.2 to 1.8, the magnitude of the order parameter stays in a small range from 0.85 to 0.89, showing that the c band has limited effects on the f band magnetic structure.

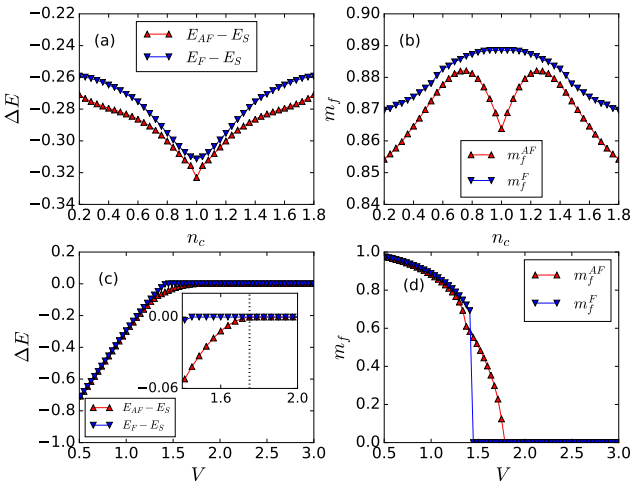

FIG. 3: MFT results away from half-filling. (a) $E_{AF}-E_S$ and E_F-E_S as a function of density n_c. (b) m_f^{AF} and m_f^F as a function of density n_c. Panels (a) (b) are fixed at $n_d=1$, $n_f=1$, $t'=1$, $V=1$, $U_f=4$ and $L=200$. (c) $E_{AF}-E_S$ and E_F-E_S as a function of hybridization strength V. The dashed line in the inset indicates the critical point V_c. (d) m_f^{AF} and m_f^F as a function of V. Panels (c) (d) are fixed at $n_c=0.8$, $n_d=1$, $n_f=1$, $t'=1$, $U_f=4$ and $L=200$.

In Fig. 3(c), $E_{AF}-E_S$ and E_F-E_S are shown as a function of the hybridization strength V with fixed $n_c=0.8$, $n_d=1$, $n_f=1$, $t'=1$, $U_f=4$ and $L=200$. Below the critical point $V_c\approx 1.75$, E_{AF} is lower than E_F and E_S. Above the critical point, the AF order gives way to the singlet phase in a second order phase transition. In Fig. 3(d), the explicit behaviours of m_f^{AF} and m_f^F with respect to V are presented, in agreement with results of Fig. 3(c). Red triangular data points characterize the behaviour of the ground state order parameter. Notably, by moving away from half-filling, the smooth transition observed at the half-filling limit returns to the conventional MFT transition behaviour with order parameter exponent $\beta=1/2$.

IV. RESULTS: DETERMINANT QUANTUM MONTE CARLO

In contrast to MFT, DQMC provides an exact treatment of the interactions in the KI-M Hamiltonian. This is accomplished through the construction of a path integral expression for the partition function and the introduction of an auxiliary field to decouple the exponential of the quartic interaction term into a quadratic form[35]. The fermion trace can be done exactly, and the auxiliary field is then sampled to produce measurements of one and two particle correlation functions.

The DQMC method works on lattices of finite spatial extent, necessitating an extrapolation to the thermodynamic limit as described below. A "Trotter error" is also introduced in the separation of the kinetic and potential energy pieces of the Hamiltonian. We work with an imaginary time discretization small enough such that the Trotter error is negligible, i.e. it is less than our statistical sampling errors. All the following DQMC results are presented at the particle-hole symmetric limit.

To explore the magnetic behaviour, we first study the f band real space equal time spin-spin correlation function,

$$C^f(\mathbf{r}) = \langle S^f_{\mathbf{i}+\mathbf{r},z}\, S^f_{\mathbf{i},z}\rangle = \langle (n^f_{\mathbf{i}+\mathbf{r}\uparrow}-n^f_{\mathbf{i}+\mathbf{r}\downarrow})(n^f_{\mathbf{i}\uparrow}-n^f_{\mathbf{i}\downarrow})\rangle \quad (8)$$

$C^f(\mathbf{r})$ measures the correlation between the z component of a spin on site $\mathbf{i}$ with that on a site a distance $\mathbf{r}$ away. Although the definition in Eq. 8 only involves the z component, we average all three components (which are equal by rotational symmetry).

In addition to the spatial decay of the f band spin correlation function of Eq. 8, we also study the Kondo singlet correlation function[41], defined as:

$$C^{fd} = \langle \vec{S}^f_{\mathbf{i}} \cdot \vec{S}^d_{\mathbf{i}}\rangle \quad (9)$$

where $\vec{S}^f_{\mathbf{i}} = [f^\dagger_{\mathbf{i}\uparrow}\ f^\dagger_{\mathbf{i}\downarrow}]\,\vec{\sigma}\begin{bmatrix} f_{\mathbf{i}\uparrow} \\ f_{\mathbf{i}\downarrow}\end{bmatrix}$ and $\vec{S}^d_{\mathbf{i}} = [d^\dagger_{\mathbf{i}\uparrow}\ d^\dagger_{\mathbf{i}\downarrow}]\,\vec{\sigma}\begin{bmatrix} d_{\mathbf{i}\uparrow} \\ d_{\mathbf{i}\downarrow}\end{bmatrix}$ and $\vec{\sigma}$ are the Pauli matrices.

At a KI-M coupling $t'=1$, the DQMC result for the f band spin-spin correlation function $C^f(\mathbf{r})$ shown in Fig. 4 reveals non-zero (long range) AF correlations

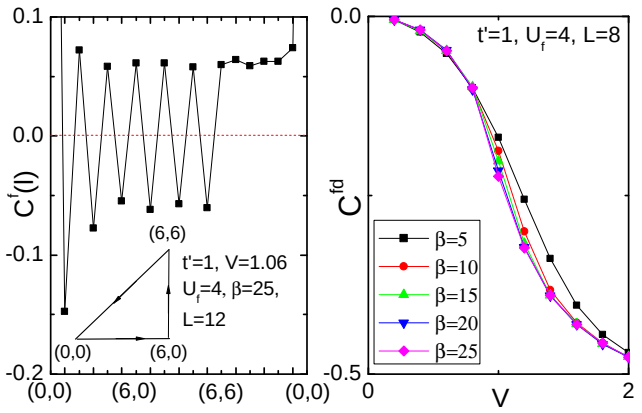

FIG. 4: Left: The equal time spin-spin correlation function as a function of distance $\mathbf{r}$, on a 12×12 lattice, with fixed $t' = 1$, $V = 1.06$, $U_f = 4$, $\beta = 25$. The horizontal axis follows the direction of the triangular path on the lattice with the AF correlations clearly present. Long range order is clearly evident, even though V exceeds the critical value V_c for the AF-singlet transition of the PAM: t' nonzero has stabilized AF. Right: The singlet correlation function C^{fd} increases in magnitude with hybridization V. Since C^{fd} measures local correlations, its reaches an asymptotic low T value at relatively small $\beta \approx 10$.

at hybridization strength $V = 1.06$. This value is well above the pure KI ($t' = 0$) critical point, indicating that AF order is stabilized by t'. The right panel of Fig. 4 shows the variation of the singlet correlation function C^{fd} with hybridization strength. As V increases, the system switches from a small C^{fd} regime where singlet correlations are absent (the AF phase dominates) to a large C^{fd} regime where Kondo singlets are well formed (and AF correlations are absent). As has been previously noted[37], the position of the most rapid increase in magnitude of C^{fd} gives an approximate location to the AF-singlet QCP.

In addition to the manner in which the spin correlation function decays with spatial separation, the imaginary time evolution also offers a window into the AF-singlet transition. Specifically, the f band dynamic local moment,

$$\langle m^2 \rangle_{\rm dyn} = \frac{1}{\beta} \int_0^\beta d\tau \, C^f(\mathbf{r} = 0, \tau) = \frac{1}{\beta} \int_0^\beta d\tau \, \langle S^f_{\mathbf{i}z}(\tau) S^f_{\mathbf{i}z}(0) \rangle \qquad (10)$$

is the integral of the spatially local, unequal time spin correlation function $C^f(\mathbf{r} = 0, \tau)$. Here $S^f_{\mathbf{i}z}(\tau) = e^{H\tau} S^f_{\mathbf{i}z} e^{-H\tau}$. As with our previous equal time $C^f(\mathbf{r})$, we average this correlation function over all spin directions to improve statistics. In a situation where the spin operator commutes with the Hamiltonian, e.g. at $V = 0$ where one has isolated moments, the instantaneous, $C^f(\mathbf{r} = 0, \tau = 0)$, and dynamic moments $\langle m^2 \rangle_{\rm dyn}$ are equal. Quantum fluctuations from the hybridization V cause the spin correlation to decay in imaginary time, reducing the dynamic moment.

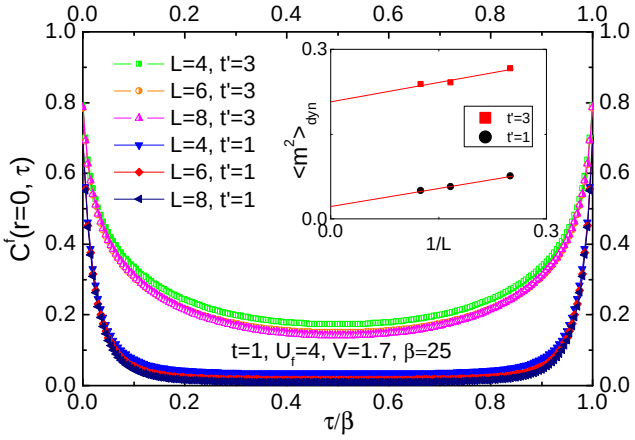

FIG. 5: The spin correlation function as a function of imaginary time separation. Here $U_f = 4$ and $V = 1.70$ are fixed. The unequal time correlation function rapidly decays to zero for $t' = 1$, while it decays smoothly to a non-zero value for $t' = 3$, suggesting the values correspond to two distinct magnetic phases. Finite size effects are verified to be small by comparing data for $L = 4, 6, 8$. This lack of dependence on L is associated with the fact that the quantity being measured is local in space. Inset: The f band dynamic local moment as a function of $1/L$. For $t' = 1$ the extrapolated local moment is $\langle m^2 \rangle_{\rm dyn} \sim 0.024$, corresponding to a screened Kondo singlet phase, while for $t' = 3$ it is almost an order of magnitude greater, $\langle m^2 \rangle_{\rm dyn} \sim 0.21$, corresponding to an ordered magnetic phase. The extrapolation was performed using a linear least-squares fit.

As seen in Fig. 5 there are two quite different behaviors of $C^f(\mathbf{r} = 0, \tau)$ when V is non-zero. $C^f(\mathbf{r} = 0, \tau)$ decays to zero rapidly at $\tau/\beta = 0.5$ for $t' = 1$, while it decays smoothly to a non-zero value at $\tau/\beta = 0.5$ for $t' = 3$. Integrating $C^f(\mathbf{r} = 0, \tau)$ yields the dynamic local moments shown in the inset to Fig. 5. Increasing t' from 1 to 3, induces a very large change in $\langle m^2 \rangle_{\rm dyn}$, which implies the shifting of the system from a Kondo singlet to an AF phase.

The rapid decay of $C^f(\mathbf{r} = 0, \tau)$ with τ is associated with the presence of a singlet gap. An alternate way of interpreting the data of Fig. 5 is that by enhancing the AF tendency, increasing t' causes the vanishing to the singlet gap and a large increase in $\langle m^2 \rangle_{\rm dyn}$.

The f-band structure factor $S^f(\mathbf{k})$ is the Fourier transform of the f-band equal time spin-spin correlation function $C^f(\mathbf{r})$, and is defined as:

$$S^f(\mathbf{k}) = \sum_{\mathbf{r}} e^{i\mathbf{k}\mathbf{r}} C^f(\mathbf{r}) \qquad (11)$$

We present results for $\mathbf{k} = \mathbf{Q}$, the AF structure factor, since this is the dominant ordering wave vector at half-filling.

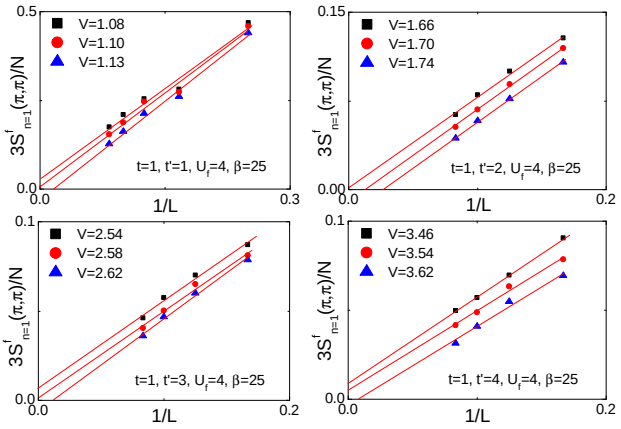

FIG. 6: Finite size scaling of the structure factor $S^f_{n=1}(\mathbf{Q})$ at $t' = 1,\ 2,\ 3,\ 4$ and fixed $U_f = 4, \beta = 25$. The subscript $n = 1$ emphasizes we exclude $C^f\big(\mathbf{r} = (0,0)\big)$ to reduce the finite size corrections. See text. The critical V above which AF order is lost (the extrapolation becomes zero) increases with t'. The extrapolation was performed using a linear least-squares fit.

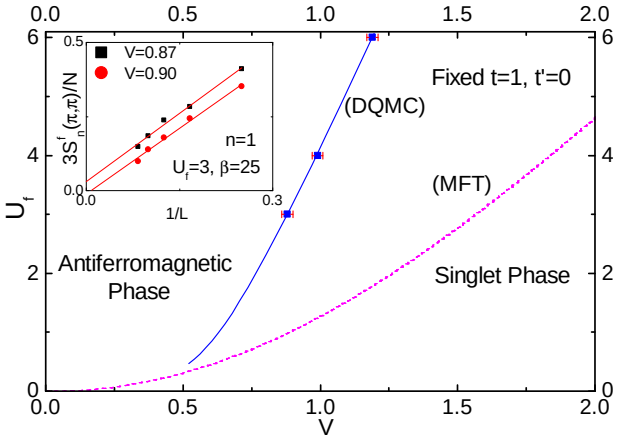

FIG. 7: The ground state U_f-V phase diagram of the half-filled PAM ($t' = 0$). The three blue squares indicate the DQMC QCP, while the dotted line shows the MFT results. The solid line is a guide to the eye. Inset: Finite size scaling of $S^f_n(\mathbf{Q})$ for $n = 1$ at $V = 0.87$ and $V = 0.90$, and $U_f = 3$, $\beta = 25$ We have set $n = 1$ corresponding to exclusion of $C\big(\mathbf{r} = (0,0)\big)$. The extrapolation was performed using a linear least-squares fit.

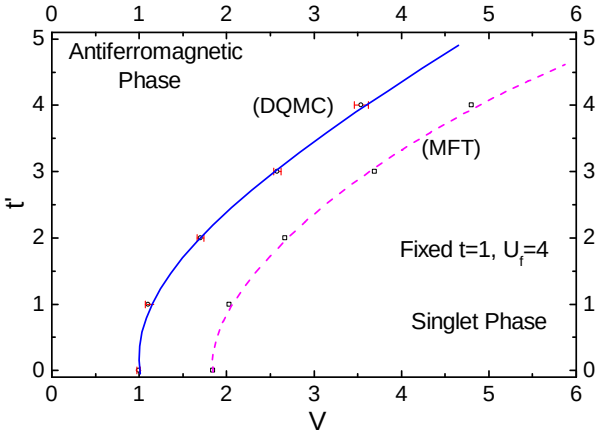

FIG. 8: The ground state t'-V phase diagram of the half-filled KI-M system at fixed $t = 1, U_f = 4$. The blue solid line indicates the DQMC boundary and the pink dotted line indicates the MFT boundary, both of which separate the AF phase and the singlet phase.

If there is long range AF order in the system, $C^f(\mathbf{r})$ remains non-zero to large separations $\mathbf{r}$ and hence the spatial sum to form $S^f(\mathbf{Q})$ yields a quantity which increases linearly with the system size N. Spin wave theory[42] provides the analytic form for the finite size correction

$$\frac{3S^f(\mathbf{Q})}{N} = \frac{a}{L} + m^2_{AF,f} \tag{12}$$

Here $m_{AF,f}$ is the AF order parameter in the thermodynamic limit and $L = \sqrt{N}$ is the linear lattice size. The correction factor a can be reduced by excluding short range terms $C^f\big(\mathbf{r} = (0,0)\big)$ from the sum used to build the full structure factor, since spin correlations at short distances are enhanced over the square of the order parameter $m_{AF,f}$. An improved estimator (lower finite size effects) is therefore[43],

$$S^f_n(\mathbf{Q}) = \frac{N}{N-n} \sum_{\mathbf{r},|r|>l_c} e^{i\mathbf{Q}\mathbf{r}} C^f(\mathbf{r}) \tag{13}$$

where n is the number of separations $\mathbf{r}$ shorter than l_c which are excluded from the sum. In our DQMC measurements, we chose $l_c = 0$ and $n = 1$, removing only the fully local spin-spin correlation $C^f(0,0)$. (This is the off-vertical scale data point in Fig. 4.)

To locate the phase transition point accurately, we measure the structure factor $S^f_n(\mathbf{Q})$ according to Eq. 12, and then extrapolate to get the order parameter $m_{AF,f}$. The results are shown in Fig. 6. Fixing $t = 1, U_f = 4, \beta = 25$, then for $t' = 1$, $m_{AF,f}$ has a negative extrapolation at $V = 1.13$, but is positive at $V = 1.08$. These bracket the QCP which we estimate to be at $V_c = 1.10 \pm 0.03$. Similarly, for $t' = 2$, we conclude $V_c = 1.70 \pm 0.04$; for $t' = 3$, we have $V_c = 2.58 \pm 0.04$; and finally for $t' = 4$, we find $V_c = 3.54 \pm 0.08$.

Although our focus here is on the KI-M model and ascertaining the effect of additional metallic bands on the AF-singlet transition, we also have determined V_c more accurately for the PAM ($t' = 0$). To our knowledge, the original DQMC results[37] have not been re-examined. The main panel of Fig. 7 shows the U_f-V phase diagram, and the AF and singlet regions at $t' = 0$. The critical points are deduced from the scaling of $S^f_n(\mathbf{Q})$. A representative plot is shown in the inset for $U_f = 3$. $V = 0.90$ (zero intercept) and $V = 0.87$ (non-zero intercept), bracket a critical value $V_c = 0.89 \pm 0.02$ at $U_f = 3$. Similarly, for $U_f = 4$, we conclude $V_c = 0.99 \pm 0.02$ and

for $U_f = 6$, we conclude $V_c = 1.18 \pm 0.02$. The dotted line showing the MFT results has been discussed in the previous section.

We now consider the phase diagram for the full KI-M Hamiltonian with $t' \neq 0$. Here we chose to fix $U_f = 4$ and focus on the effect of coupling the KI to the metal with t'. The phase diagram is shown in Fig. 8. With the increase of t', the critical value V_c increases in both DQMC and MFT calculations, quantifying the degree to which interlayer hopping parameter t' enhances the RKKY interaction and stabilizes the AF phase. The increase in V_c is quite substantial. In contrast, previous comparisons[44] of the PAM with on-site (insulating) and intersite (metallic) d f hybridization did not reveal as great a difference in V_c. This suggests the increase found here is associated with the van-Hove singularity in the DOS.

V. SPECTRAL FUNCTION AND DYNAMIC SPIN STRUCTURE FACTOR

DQMC is also able to evaluate (real time) dynamic information through analytic continuation[45] of the imaginary time correlation function. Inverting the integral relation,

$$G_\alpha(\mathbf{q},\tau) = \int_{-\infty}^{+\infty} d\omega \frac{e^{-\omega\tau}}{1+e^{-\beta\omega}} A_\alpha(\mathbf{q},\omega) \qquad (14)$$

yields the spectral function from the one particle Greens functions measured in DQMC. Here $\alpha = c, d, f$ labels the band. The associated densities of states are given by $\rho_\alpha(\omega) = \sum_{\mathbf{q}} A_\alpha(\mathbf{q},\omega)$. The low frequency behavior of $\rho_\alpha(\omega)$ quantifies the possible existence of Slater, Mott, or hybridization gaps.

The dynamic spin structure factor is similarly related to an imaginary time counterpart which is a generalization of the quantity of Eq. 10 to include intersite correlations,

$$\chi_\alpha(\mathbf{q},\tau) = \frac{1}{N}\sum_{\mathbf{j},\mathbf{l}} e^{i\mathbf{q}(\mathbf{j}-\mathbf{l})} \langle S^\alpha_{\mathbf{j}_z}(\tau) S^\alpha_{\mathbf{l}_z}(0)\rangle$$

$$\chi_\alpha(\mathbf{q},\tau) = \frac{1}{\pi}\int_{-\infty}^{+\infty} d\omega \frac{e^{-\omega\tau}}{1-e^{-\beta\omega}} \mathrm{Im}\chi_\alpha(\mathbf{q},\omega) \qquad (15)$$

In an AF ordered phase, the presence of low energy spin wave excitations leads to a vanishing of the gap in $\mathrm{Im}\chi_\alpha(\mathbf{q},\omega)$ at the ordering wave vector (in our case $\mathbf{Q} = (\pi,\pi)$).

In Fig. 9 and Fig. 10, we show the one particle spectral function $A_f(\mathbf{q},\omega)$ and the spin spectral function $\mathrm{Im}\chi_f(\mathbf{q},\omega)$, which are calculated using the maximum entropy method[46,47], for the PAM model and the KI-M model respectively. $\mathrm{Im}\chi_f(\mathbf{q},\omega)$ complements the data for the equal time spin and singlet correlators of Fig. 4. In their AF phases (left panels) the PAM and the KI-M models are both characterized by a single particle gap in $A_f(\mathbf{q},\omega)$. $\mathrm{Im}\chi_f(\mathbf{q},\omega)$ has a finite spectral weight (no gap) near $\omega = 0$ indicating the presence of low energy spin wave excitations in an AF phase. As has previously been noted in DQMC[37] in the singlet phase of the PAM, a spin gap opens in $\mathrm{Im}\chi_f(\mathbf{q},\omega)$. Figure 11 gives the momentum integrated $\mathrm{Im}\chi_f(\omega)$. The similarity

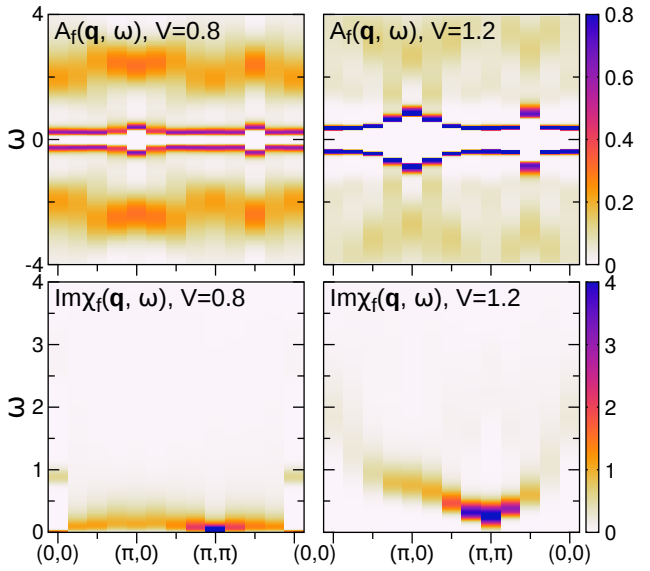

FIG. 9: Top row: The one particle spectral function $A_f(\mathbf{q},\omega)$ of the PAM in the presence (left) and absence (right) of AF order. Bottom row: Spin spectral function $\mathrm{Im}\chi_f(\mathbf{q},\omega)$. Results are computed on an $N = 8\times 8$ cluster at fixed $t = 1, U_f = 4, \beta = 25$.

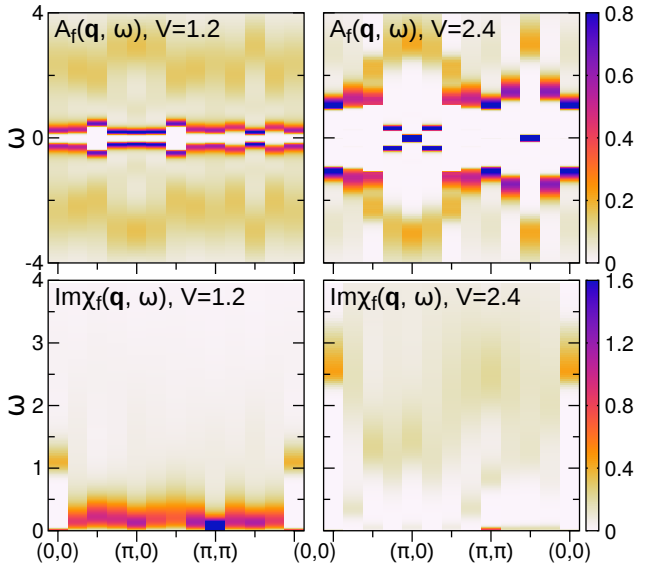

FIG. 10: Top row: The one particle spectral function $A_f(\mathbf{q},\omega)$ of the KI-M in the presence (left) and absence (right) of AF order. Bottom row: Spin spectral function $\mathrm{Im}\chi_f(\mathbf{q},\omega)$. Results are computed on an $N = 8\times 8$ cluster at fixed $t = 1, t' = 2, U_f = 4, \beta = 25$.

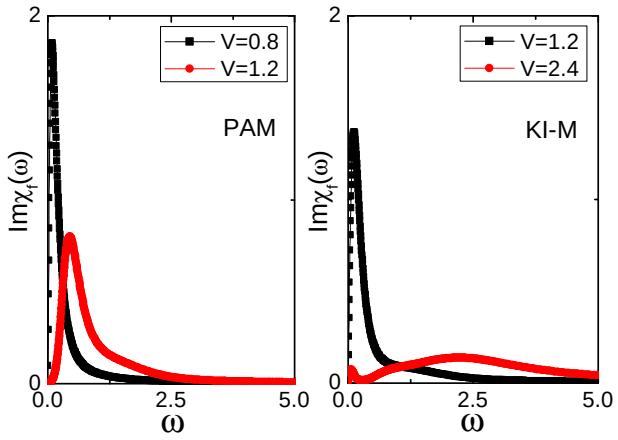

FIG. 11: Left: The dynamic spin structure factor $\mathrm{Im}\chi_f(\omega)$ of the PAM at fixed $t = 1, U_f = 4, \beta = 25$. Right: The dynamic spin structure factor $\mathrm{Im}\chi_f(\omega)$ of the KI-M at fixed $t = 1, t' = 2, U_f = 4, \beta = 25$. Both results are calculated on $N = 8 \times 8$ clusters.

between the PAM and KI-M is clear, although the singlet phase dynamic spin response of the KI-M is considerably broader, a natural consequence of the larger value of V required to destroy AF order and of the hybridization to an additional band.

The singlet phase of the KI-M is distinguished from the PAM by a non-zero $A_f(\mathbf{q}, \omega)$ at $\omega = 0$ and also a very broadly distributed spectral weight $\mathrm{Im}\chi_f(\mathbf{q}, \omega)$ (Fig. 10, bottom right). The distinction between the singlet phases of the KI-M and the PAM is further confirmed by the dynamic spin structure factors, given by $\mathrm{Im}\chi_f(\omega) = \sum_{\mathbf{q}} \mathrm{Im}\chi_f(\mathbf{q}, \omega)$ for both models, as shown in Fig. 11.

VI. CONCLUSIONS

A considerable body of existing theoretical and numerical work[27,49–54] has examined coupling of a single band Hubbard model to additional conduction electrons as a model of metal-insulator interfaces, and the possibility of penetration of AF and Mott insulator features of strong interaction into the metal, and *vice-versa*. Qualitative similarities exist between phenomena like singlet formation between electrons in distinct bands and between electrons in two conjoined materials. In this paper we have first shown that within a self-consistent MFT there is a tendency towards expansion of the region of AF stability in a three band extension of the PAM.

We next employed the DQMC method to confirm these findings with an exact, beyond MF, treatment of the correlations, and thereby identify quantitatively the critical f d hybridization in the plane of interaction strength U_f and hopping t' between the PAM and the metal. In the process, we improved on the previously known V_c in the PAM ($t' = 0$) limit. Our primary observables in the characterization of the phases were the AF structure factor, the singlet correlator, and the dynamical moment, which all provide a consistent picture of the location of the phase boundary. Work within DMFT[29], which focuses on the paramagnetic phase, is complementary to what we have done here.

Although the AF phase of the KI-M is stabilized by contact with the metal, the behavior of $\mathrm{Im}\chi_f(\mathbf{q}, \omega)$ is not dramatically different from the PAM. $\mathrm{Im}\chi_f(\mathbf{q}, \omega)$ has a gap Δ_s at low freqencies in the singlet phase, but has non-zero low frequency spectral weight in the AF phase associated with spin-wave excitations.

In contrast, the single particle spectral weight $A_f(\mathbf{q}, \omega)$, and the momentum-integrated density of states, behave differently in the KI-M than the PAM. The PAM has a nonzero charge gap Δ_c in both the AF and singlet phases[37], with $\Delta_s/\Delta_c \to 1$ as V increases to deep in the singlet phase. We find here that for the KI-M there are peaks in $A(\mathbf{q}, \omega)$ near $\mathbf{q} = (\pi, 0)$ and $\mathbf{q} = (\pi/2, \pi/2)$ and hence also in $\rho_f(\omega) = \sum_{\mathbf{q}} A_f(\mathbf{q}, \omega)$. We believe this distinction to originate in the fact that even though the AF order is lost, the additional c-electrons still strongly interact with the d and f bands of the KI, so that there is no longer an insulating Kondo gap.

The Hamiltonian, Eq. 1 includes cd and df hybridizations. We have also done some studies of the effect of on-site cf hopping. In order to keep the lattice bipartite and avoid a sign problem we have altered the df hybridization to a near-neighbor form also used, for example, in[44]. This change does not shift the critical V from the on-site value, to within our error bars. Having verified this, we then added cf hopping and find that it, also, leaves the critical point at the same value. We conclude that more complex (and realistic) forms of the electronic kinetic energy have little effect on the qualitative and quantitative results of our paper: an enhancement of the regime of AF order.

Our work on a two layer metal-PAM represents a first step in the application of DQMC to the more general investigation of f-electron-metal superlattices, where, on the experimental side, dimensionality can be controlled[28]. Theoretical and numerical studies within dynamical mean field theory[29,55–57] of these structures have already led to great insight. Including the full spatial structure of each layer, as done in DQMC, makes the full superlattice problem challenging.

Acknowledgments

We acknowledge N.C. Costa for useful discussions. WH and RTS at UC-Davis were supported by the U.S. Department of Energy under grant number DE-SC0014671. EWH and BM at Stanford/SLAC, primarily for the analytic continuation and its interpretation, were supported by the U.S. Department of Energy (DOE), Office of Basic Energy Sciences, Division of Materials Sciences and Engineering, under Contract No. DE-

AC02-76SF00515.

[1] "Localized Magnetic States in Metals", P W. Anderson, Phys. Rev. 124, 41 (1961).

[2] "Heavy-fermion systems", G.R. Stewart, Rev. Mod. Phys. 56, 755 (1984).

[3] "Theories of heavy-electron systems", P.A. Lee, T.M. Rice, J.W. Serene, L.J. Sham, and J.W. Wilkins, Comments Condens. Matt. Phys. 12, 99 (1986).

[4] "Dynamical mean-field theory of strongly correlated fermion systems and the limit of infinite dimensions", A. Georges, G. Kotliar, W. Krauth, and M.J. Rozenberg, Rev. Mod. Phys. 68, 13 (1996).

[5] "Dynamics and scaling in the periodic Anderson model", N.S. Vidhyadhiraja and D E. Logan, Eur. Phys. J. B 39, 313 (2004).

[6] "Quantum critical Mott transitions in a bilayer Kondo insulator-metal model system", S. Sen and N. S. Vidhyadhiraja, Phys. Rev. B 93, 155136 (2016).

[7] A.C. Hewson, *The Kondo Problem to Heavy Fermions*, (Cambridge University Press, Cambridge, 1993).

[8] "DMFT Study for Valence Fluctuations in the Extended Periodic Anderson Model", R. Shinzaki, J. Nasu, and A. Koga: J. Phys. Conf. Ser. 683, 012041 (2016).

[9] "Kondo Volume Collapse and the $\gamma \rightarrow \alpha$ Transition in Cerium", J.W. Allen and R.M. Martin, Phys. Rev. Lett. 49, 1106 (1982).

[10] "$\alpha \rightarrow \gamma$ transition in Ce. II. A detailed analysis of the Kondo volume-collapse model", J.W. Allen and L.Z. Liu, Phys. Rev. B 46, 5047 (1992).

[11] "Volume collapse in the Kondo lattice", M. Lavagna, C. Lacroix, and M. Cyrot, Phys. Lett. A 90, 210 (1982).

[12] "Electron spectroscopies for Ce compounds in the impurity model", O. Gunnarsson and K. Schonhammer, Phys. Rev. B 28, 4315 (1983).

[13] "Volume Collapse transitions in the rare earth metals," A. McMahan, C. Huscroft, R.T. Scalettar, and E.L. Pollock, J. Comput.-Aided Mater. Des. 5, 131 (1998).

[14] "Thermal Signatures of the Kondo Volume Collapse in Cerium" M.J. Lipp, D. Jackson, H. Cynn, C. Aracne, W.J. Evans, and A.K. McMahan, Phys. Rev. Lett. 101, 165703 (2008).

[15] "4f electron delocalization and volume collapse in praseodymium metal," J.A. Bradley, K.T. Moore, M.J. Lipp, B.A. Mattern, J.I. Pacold, G.T. Seidler, P. Chow, E. Rod, Y. Xiao, and W.J. Evans Phys. Rev. B 85, 100102(R) (2012).

[16] "Phase Diagram and Electronic Structure of Praseodymium and Plutonium," N. Lanatá, Y. Yao, C-Z. Wang, K-M. Ho, and G. Kotliar, Phys. Rev. X 5, 011008 (2015).

[17] "Pairing correlations near a Kondo-destruction quantum critical point," J.H. Pixley, L. Deng, K. Ingersent, and Q. Si, Phys. Rev. B 91, 201109(R) (2015).

[18] "Indirect Exchange Coupling of Nuclear Magnetic Moments by Conduction Electrons", M.A. Ruderman and C. Kittel, Phys. Rev. 96, 99 (1954).

[19] "A Theory of Metallic Ferro- and Antiferromagnetism on Zener's Model", T. Kasuya, Prog. Theor. Phys. 16, 45 (1956).

[20] "Magnetic Properties of Cu-Mn Alloys", K. Yosida, Phys. Rev. 106, 893 (1957).

[21] "Theory of Dilute Magnetic Alloys", J. Kondo, Solid State Phys. 23, 183 (1969).

[22] "Revival of the Kondo effect", L. Kouwenhoven and L. Glazman, Phys. World 14, No. 1, 33-38 (2001).

[23] J. Mannhart and D.G. Schlom, in *Thin Films and Heterostructures for Oxide Electronics*, edited by S. ogale (Springer, New York, 2005), p25.

[24] "Oxide Interfaces- An Opportunity for Electronics", J. Mannhart and D.G. Schlom, Science 327, 1607 (2010).

[25] A. Millis, in *Thin Films and Heterostructures for Oxide Electronics*, edited by S. Ogale (Springer, New York, 2005), p279.

[26] J.K. Freericks, *Transport in Multilayers Nanostructures: The Dynamical Mean Field Theory Approach*, (Imperial College Press, London, 2006).

[27] "Kondo Screening and Magnetism at Interfaces," A. Euverte, F. Hébert, S. Chiesa, R.T. Scalettar, and G. G. Batrouni, Phys. Rev. Lett. 108, 246401 (2012)

[28] "Tuning the Dimensionality of the Heavy Fermion Compound $CeIn_3$", H. Shishido, T. Shibauchi, K. Yasu, T. Kato, H. Kontani, T. Terashima, and Y. Matsuda, Science 327, 980 (2010).

[29] "Kondo effect in f-electron superlattices," R. Peters, Y. Tada, and N. Kawakami, Phys. Rev. B 88, 155134 (2013).

[30] "Single Mott transition in the multiorbital Hubbard model", A. Liebsch, Phys. Rev. B 70, 165103 (2004).

[31] "Orbital-selective Mott-Hubbard transition in the two-band Hubbard model", R. Arita and K. Held, Phys. Rev. B 72, 201102(R) (2005).

[32] "Periodic Anderson model with electron-phonon correlated conduction band", P. Zhang, P. Reis, K. Tam, M. Jarrell, J. Moreno, F. Assaad, and A. K. McMahan, Phys. Rev. B 87, 121102(R) (2013).

[33] "Spectral changes in layered f-electron systems induced by Kondo hole substitution in the boundary layer", S. Sen, J. Moreno, M. Jarrell, and N.S. Vidhyadhiraja, Phys. Rev. B 91, 155146 (2015).

[34] "Finite f-electron Bandwidth in a Heavy Fermion Model", A. Euverte, S. Chiesa, R.T. Scalettar, and G.G. Batrouni, Phys. Rev. B 88, 235123 (2013).

[35] "Monte Carlo calculations of coupled boson-fermion systems. I", R. Blankenbecler, D.J. Scalapino, and R.L. Sugar, Phys. Rev. D 24, 2278 (1981).

[36] E. Loh and J. Gubernatis, in Modern Problems of Condensed Matter Physics, edited by W. Hanke and Y. V. Kopaev (North Holland, Amsterdam, 1992), Vol. 32, p. 177.

[37] "Competition Between Antiferromagnetic Order and Spin Liquid Behavior in the Two–Dimensional Periodic Anderson Model at Half–Filling," M. Vekic, J.W. Cannon, D.J. Scalapino, R.T. Scalettar, and R.L. Sugar, Phys. Rev. Lett. 74, 2367 (1995).

[38] "Coexistence of magnetic order and Kondo effect in the Kondo-Heisenberg model", B.H. Bernhard and C. Lacroix, Phys. Rev. B92, 094401 (2015).

[39] "Antiferromagnetic phases of the Kondo lattice," R. Eder,

K. Grube, and P. Wróbel, Phys. Rev. B93, 165111 (2016).
[40] "Spiral magnetic phases on the Kondo Lattice Model: A HartreeFock approach", N.C. Costaa, J.P. Limab and R. R. dos Santosa, Journal of Magnetism and Magnetic Materials 423 (2017).
[41] "Magnetic and Thermodynamic Properties of the Three-Dimensional periodic Anderson Hamiltonian," C. Huscroft, A.K. McMahan, and R.T. Scalettar, Phys. Rev. Lett. 82, 2342 (1999).
[42] "Ground-state staggered magnetization of two-dimensional quantum Heisenberg antiferromagnets", D.A. Huse, Phys. Rev. B 37, 2380 (1988).
[43] "Quantum Monte Carlo Study of the 2D Fermion Hubbard Model at Half-Filling," C.N. Varney, C.-R. Lee, Z.J. Bai, S. Chiesa, M. Jarrell, and R.T. Scalettar, Phys. Rev. B 80, 075116 (2009).
[44] "Similarities between the Hubbard and Periodic Anderson Models at Finite Temperatures", K. Held, C. Huscroft, R.T. Scalettar, and A.K. McMahan, Phys. Rev. Lett. **85**, 373 (2000).
[45] "Bayesian inference and the analytic continuation of imaginary-time quantum Monte Carlo data", M. Jarrell and J.E. Gubernatis, Phys. Rep. 269, 135 (1996).
[46] "Quantum Monte Carlo simulations and maximum entropy: Dynamics from imaginary-time data", J. E. Gubernatis, M. Jarrell, R. N. Silver, and D. S. Sivia, Phys. Rev. B 44, 6011 (1991).
[47] "Identifying the maximum entropy method as a special limit of stochastic analytic continuation", K. S. D. Beach, arXiv:cond-mat/0403055.
[48] "Artificial Charge-Modulation in Atomic-Scale Perovskite Titanate Superlattices", A. Ohmoto, D. Muller, J. Grazul, and H. Hwang, Nature (London) 419, 378 (2002).
[49] "Metallic surface of a Mott insulatorMott insulating surface of a metal", M. Potthoff and W. Nolting, Phys. Rev. B 60, 7834 (1999).
[50] "Surface metal-insulator transition in the Hubbard model", M. Potthoff and W. Nolting, Phys. Rev. B 59, 2549 (1999).
[51] "Spatial inhomogeneity and strong correlation physics: A dynamical mean-field study of a model Mott-insulator-band-insulator heterostructure", S. Okamoto and A.J. Millis, Phys. Rev. B 70, 241104 (2004).
[52] "Charge-Orbital Density Wave and Superconductivity in the Strong Spin-Orbit Coupled IrTe2Pd", H. Zenia, J.K. Freericks, H.R. Krishnamurthy, and T. Pruschke, Phys. Rev. Lett. 103, 116402 (2009).
[53] "First-order metal-to-metal phase transition and non-Fermi-liquid behavior in a two-dimensional Mott insulating layer adsorbed on a metal substrate", H. Ishida and A. Liebsch, Phys. Rev. B 85, 045112 (2012).
[54] "Kondo Proximity Effect: How Does a Metal Penetrate into a Mott Insulator?", R.W. Helmes, T.A. Costi, and A. Rosch, Phys. Rev. Lett. 101, 066802 (2008).
[55] "Enhanced Superconductivity in Superlattices of High-Tc Cuprates", S. Okamoto and T.A. Maier, Phys. Rev. Lett. 101, 156401 (2008).
[56] "Dimensional crossover in layered f-electron superlattices", Y. Tada, R. Peters, and M. Oshikawa, Phys. Rev. B 88, 235121 (2013).
[57] "Surface density of states of layered f-electron materials", R. Peters and N. Kawakami, Phys. Rev. B 89, 041106 (2014).